The Astrophysical Journal, 656:666–679, 2007 February 20

THE KECK+MAGELLAN SURVEY FOR LYMAN LIMIT ABSORPTION. I. THE FREQUENCY DISTRIBUTION OF SUPER LYMAN LIMIT SYSTEMS[1]

John M. O'Meara,[2] Jason X. Prochaska,[3,4] Scott Burles,[5] Gabriel Prochter,[3,4]
Rebecca A. Bernstein,[6] and Kristin M. Burgess[7]

Received 2006 August 10; accepted 2006 October 29

ABSTRACT

We present the results of a survey for super Lyman limit systems (SLLSs; defined to be absorbers with 19.0 cm^{-2} $\leq$ log $N_{\rm H\,I} \leq$ 20.3 cm^{-2}) from a large sample of high-resolution spectra acquired using the Keck and Magellan telescopes. Specifically, we present 47 new SLLSs from 113 QSO sight lines. We focus on the neutral hydrogen frequency distribution $f_{\rm H\,I}(N, X)$ of the SLLS and its moments and compare these results with the Lyα forest and the damped Lyα systems (DLAs; absorbers with log $N_{\rm H\,I} \geq$ 20.3 cm^{-2}). We find that the $f_{\rm H\,I}(N, X)$ of the SLLSs can be reasonably described with a power law of index $\alpha = -1.43^{+0.15}_{-0.16}$ or $-1.19^{+0.20}_{-0.21}$ depending on whether we set the lower $N_{\rm H\,I}$ bound for the analysis at $10^{19.0}$ or $10^{19.3}$ cm^{-2}, respectively. The results indicate a flattening in the slope of $f_{\rm H\,I}(N, X)$ between the SLLSs and DLAs. We find little evidence for redshift evolution in the shape of $f_{\rm H\,I}(N, X)$ for the SLLSs over the redshift range of the sample $1.68 < z < 4.47$ and only tentative evidence for evolution in the zeroth moment of $f_{\rm H\,I}(N, X)$, the line density $\ell_{\rm SLLS}(X)$. We introduce the observable distribution function $\mathcal{O}(N, X)$ and its moment, which elucidates comparisons of H I absorbers from the Lyα forest through to the DLA. We find that a simple three-parameter function can fit $\mathcal{O}(N, X)$ over the range 17.0 cm^{-2} $\leq$ log $N_{\rm H\,I} \leq$ 22.0 cm^{-2}. We use these results to predict that $f_{\rm H\,I}(N, X)$ must show two additional inflections below the SLLS regime to match the observed $f_{\rm H\,I}(N, X)$ distribution of the Lyα forest. Finally, we demonstrate that SLLSs contribute a minor fraction ($\approx$15%) of the universe's hydrogen atoms and, therefore, an even smaller fraction of the mass in predominantly neutral gas.

Subject headings: intergalactic medium — quasars: absorption lines

Online material: color figures

1. INTRODUCTION

For nearly three decades, the study of absorption-line systems toward distant quasars has addressed a wide range of astrophysical and cosmological issues. These systems are typically classified according to their neutral hydrogen content: the Lyα forest absorbers with log $N_{\rm H\,I} \leq$ 17.2 cm^{-2}, the Lyman limit systems (LLSs) with 17.2 cm^{-2} $\leq$ log $N_{\rm H\,I} \leq$ 20.3 cm^{-2}, and the damped Lyα systems (DLAs) with log $N_{\rm H\,I} \geq$ 20.3 cm^{-2}. Both the Lyα forest and DLA absorbers have received considerable attention. The Lyα forest can be used to constrain cosmological parameters through a number of methods, such as through studies of the flux power spectrum (Croft et al. 2002; McDonald et al. 2005), the mean flux decrement (Tytler et al. 2004), or the distribution in column density and velocity width of the absorbers (e.g., Kirkman & Tytler 1997; Kim et al. 2002). The DLAs trace the bulk of the neutral gas at high redshift and are believed to be the progenitors of modern-day galaxies (Wolfe et al. 2005). Large statistical samples of both the Lyα forest and the DLAs are readily observed because their $N_{\rm H\,I}$ is easily determined. For the Lyα forest, the $N_{\rm H\,I}$ is determined directly from Voigt profile fits to the Lyα line, which is dominated by the Maxwellian profile, or from higher order Lyman transitions when Lyα is saturated. For the DLA, the Lorentzian component of the Voigt profile gives pronounced damping wings, allowing for accurate $N_{\rm H\,I}$ determinations from spectra even at low signal-to-noise ratio (S/N) or resolution.

Recently, Prochaska et al. (2005, hereafter PHW05) analyzed the thousands of spectra from the Sloan Digital Sky Survey (SDSS) Data Release 3 and determined the $N_{\rm H\,I}$ frequency distribution for over 500 DLAs. In contrast, there exists comparatively little study of the LLSs. Surveys for LLS absorption (Tytler 1982; Sargent et al. 1989; Lanzetta 1991; Storrie-Lombardi et al. 1994; Stengler-Larrea et al. 1995) have concentrated primarily on the frequency of absorption with redshift [frequently expressed as dn/dz or dN/dz, but we adopt the notation $\ell(z)$ for the line density that was introduced by PHW05], but not on the $N_{\rm H\,I}$ value of the LLS. These surveys generally included the full range of H I column density of log $N_{\rm H\,I} \geq$ 17.2 cm^{-2} in $\ell(z)$. As such, the surveys also contained the $\ell(z)$ of DLAs.

Our ignorance of LLSs largely stems from the fact that accurate determinations of $N_{\rm H\,I}$ for the LLSs are difficult compared to the Lyα forest and the DLAs. In part, this is because the LLSs represent the flat portion of the curve of growth for the Lyα transition and a precise $N_{\rm H\,I}$ measurement requires high-resolution observations (e.g., Steidel 1990). For most LLSs, the $N_{\rm H\,I}$ is determined by using the information from the Lyman limit, either by looking at the differential flux level above and below the limit, or by the spacing of the lines as they approach the Lyman limit, or both (e.g., Burles & Tytler 1998). The differential flux method requires a detailed understanding of the continuum flux level, which is difficult to obtain in high-redshift QSOs, and the line spacing technique requires a precise model for the hydrogen velocity structure, which can generally only be inferred from the metal lines associated with the LLSs (e.g., Kirkman et al. 2003).

[1] This paper includes data gathered with the 6.5 m Magellan Telescopes located at Las Campanas Observatory, Chile.

[2] Department of Physics, Penn State Worthington Scranton, Dunmore, PA.
[3] Department of Astronomy and Astrophysics, UCO/Lick Observatory, University of California, Santa Cruz, CA.
[4] Visiting Astronomer, W. M. Keck Observatory, which is a joint facility of the University of California, the California Institute of Technology, and NASA.
[5] MIT Kavli Institute for Astrophysics and Space Research, Massachusetts Institute of Technology, Cambridge, MA.
[6] Department of Astronomy, University of Michigan, Ann Arbor, MI.
[7] Department of Physics, Princeton University, Princeton, NJ.

These challenges are particularly acute for low-resolution observations where the Lyman series is poorly resolved.

Because the frequency of intersecting an LLS is observed to be of order one per sight line at redshifts $z > 2.5$ (Storrie-Lombardi et al. 1994), a relatively large QSO sample is required in comparison with Lyα forest studies. At redshifts $z > 3.25$, the SDSS provides just such a sample (Adelman-McCarthy et al. 2006), offering many thousands of sight lines suitable for analysis of LLSs. Unfortunately, the SDSS spectra are of too poor a resolution to provide useful constraints on the $N_{\rm H\,I}$ for the LLSs that are optically thick, i.e., $\log N_{\rm H\,I} \geq 17.5$ cm^{-2}. To address this nearly three decade gap in $N_{\rm H\,I}$, we have pursued a high-resolution survey for LLSs using telescopes in both the Northern and Southern Hemispheres. The goal of this survey is to obtain high-resolution, high-S/N spectra of at least 100 LLSs, with full coverage over the LLS $N_{\rm H\,I}$ range. In this paper we discuss a subsample of this survey, namely, the LLSs with $\log N_{\rm H\,I} \geq 19.0$ cm^{-2}. The lower bound on $N_{\rm H\,I}$ is chosen such that systems with this column density can be easily identified and analyzed in moderate- to high-resolution data (FWHM < 50 km s^{-1}; Dessauges-Zavadsky et al. 2003). The $N_{\rm H\,I}$ values for these LLSs are determined from the damping wings present in the Lyα line, in a fashion analogous with DLA analysis in lower resolution spectra. Previous work on this subset of the LLS population referred to the absorption systems as "sub-DLAs." Because the majority of these absorbers are likely to be predominantly ionized (e.g., Viegas 1995; Prochaska 1999), we adopt the nomenclature of Prochaska & Herbert-Fort (2004) for those LLSs exhibiting $\log N_{\rm H\,I} \geq 19.0$ cm^{-2}: the "super Lyman limit system" or SLLS absorbers.

The fundamental measure of a class of quasar absorption line (QAL) systems is the H I column density frequency distribution $f_{\rm H\,I}(N, X)$, defined to be the number of absorbers in the column density interval $(N, N + dN)$ identified along the cosmological distance interval $(X, X + dX)$, with $dX \equiv [H_0/H(z)](1+z)^2\, dz$. This quantity, the absorption distance, is generally evaluated across a redshift interval Δz. The $f_{\rm H\,I}(N, X)$ distribution for QAL systems is analogous to the luminosity function of galaxy surveys. Moments of $f_{\rm H\,I}(N, X)$ give important quantities such as the line density of absorption systems and the mass density of H I atoms. The $f_{\rm H\,I}(N, X)$ distribution is the starting point for assessing the baryonic mass density of these absorbers, as well as their cosmological metal budget. The frequency distribution of LLSs is of particular interest because the $N_{\rm H\,I} = 10^{17}$–10^{20} cm^{-2} interval is expected to include the $N_{\rm H\,I}$ value where QAL systems transition from primarily neutral gas to predominantly ionized gas (e.g., Zheng & Miralda-Escudé 2002; PHW05). Furthermore, Prochaska et al. (2006) have argued that the LLSs can constitute a considerable fraction of the metals in the young universe (see also Péroux et al. 2006). At $z \simeq 2$, a census for metals that includes the DLA, stars in high-z galaxies, and the intergalactic medium falls short by up to 70% of the total predicted metal mass density (e.g., Bouché et al. 2006).

The primary goal for this study of the SLLS is to extend the statistics we use to describe the Lyα forest and the DLA into regions of H I column density that are currently poorly constrained (see also Péroux et al. 2003a, 2005). By doing so, we hope to place the SLLS within the larger framework of high-redshift QSO absorption line systems and to explore their cosmological significance. Future papers will examine the ionization state, chemical abundances, and other physical properties of these absorbers. Throughout the paper we adopt values of the cosmological parameters consistent with the latest *Wilkinson Microwave Anisotropy Probe* (*WMAP*) results (Bennett et al. 2003): $\Omega_\Lambda = 0.7$, $\Omega_m = 0.3$, and $H_0 = 70$ km s^{-1} Mpc^{-1}.

2. SPECTROSCOPIC SAMPLE

The quasar sample in this paper includes spectra from two instruments, the Magellan Inamori Kyocera Echelle (MIKE; Bernstein et al. 2003) high-resolution spectrograph on the Magellan 6.5 m telescope at Las Campanas Observatory in Chile, and the Echellete Spectrograph and Imager (ESI; Sheinis et al. 2002) on the Keck II 10 m telescope in Hawaii. MIKE is a double echelle spectrograph, with a dichroic optical element splitting the beam into blue and red arms, each with their own CCD. MIKE provides full wavelength coverage, without spectral gaps from 3350 to 9500 Å in the default configuration. When a 1.0″ slit is used, MIKE has $R = 28{,}000$ and 22,000 for the blue and red sides, respectively. ESI is a spectrograph and imager, which provides continuous wavelength coverage from 3900 to 10900 Å in echellette mode. When a 0.5″ slit is used, ESI provides $R \approx 9000$.

In Table 1 we list the 57 QSOs in the current MIKE sample. For each QSO in the sample, the data were reduced using the MIKE reduction pipeline[8] (S. Burles et al. 2007, in preparation). The pipeline flat-fields, optimally extracts, flux-calibrates, and combines exposures to produce a single spectrum for the red and blue CCDs of MIKE. In Table 2 we list the 56 QSOs in the ESI sample. The bulk of these spectra come from the survey for DLA absorption presented by Prochaska et al. (2003) and are supplemented by a new sample of SDSS spectra. All of the ESI data were reduced with the ESIRedux pipeline[9] (Prochaska et al. 2003). The difference in native resolution of the two data sets will have implications for the $N_{\rm H\,I}$ completeness limit of each survey. This is discussed in greater detail in the following sections.

2.1. *UVES Sample*

In addition to the MIKE and ESI data, we include the results of the surveys by Péroux et al. (2003a, 2005), which we refer to here as the "UVES sample." All of these data were drawn from a heterogeneous sample of high-resolution observations using the UVES spectrometer (Dekker et al. 2000) on the VLT-2 telescope. In five cases, there is an overlap in quasars observed between our sample and the UVES sample. In these cases, we remove those quasars that contribute the smaller redshift path to the total sample.

2.2. *Redshift Path*

For each quasar in our sample, we define a redshift interval $\Delta z = z_{\rm end} - z_{\rm start}$ to construct the redshift path in a manner similar to that presented by PHW05. The starting redshift $z_{\rm start}$ is given by the lowest redshift at which we could identify strong Lyα features. For the majority of sight lines, this is set by the starting wavelength of the spectrum λ_0: $z_{\rm start} = \lambda_0/1215.67$ Å $- 1$. Higher values for $z_{\rm start}$ were adopted for a sight line either when there was intervening LLS absorption that completely removes the QSO flux or when the S/N of the QSO became so low as to significantly impact the likelihood of detecting a strong Lyα feature. The ending redshift $z_{\rm end}$ is given by $z_{\rm end} = 0.99 z_{\rm em} - 0.01$, where $z_{\rm em}$ corresponds to the QSO redshift. Thus, $z_{\rm end}$ is defined to be located $\approx$3000 km s^{-1} blueward of the QSO Lyα emission line. This offset was chosen to remove those LLSs that could be associated with the QSO. Tables 1 and 2 list $z_{\rm start}$ and $z_{\rm end}$ for each QSO in our sample. Also given in Tables 1 and 2 are the redshifts, $z_{\rm DLA}$, of any DLA known to be present in the data prior to the observations. It is our expectation that SLLSs are strongly clustered with DLAs (e.g., Prochaska & Wolfe 1999),

[8] See http://www.lco.cl/lco/magellan/instruments/MIKE/index.html.
[9] See http://www2.keck.hawaii.edu/inst/esi/ESIRedux/index.html.

TABLE 1
MIKE Quasar Sample

Name	R.A. (J2000.0)	Decl. (J2000.0)	z_{em}	z_{start}	z_{end}	z_{mask}[a]
Q0001−2340	00 03 45.00	−23 23 46.5	2.262	1.780	2.228	2.187
Q0101−304	01 03 55.30	−30 09 46.0	3.137	1.941	3.095	...
SDSS 0106+0048	01 06 19.24	+00 48 23.3	4.433	2.997	4.378	...
SDSS 0124+0044	01 24 14.80	+00 45 36.2	3.807	2.292	3.758	...
SDSS 0147−1014	01 45 16.59	−09 45 17.3	2.138	1.797	2.106	...
SDSS 0209−0005	02 09 50.70	−00 05 06.4	2.856	1.879	2.816	2.523
SDSS 0244−0816	02 44 47.78	−08 16 06.1	4.047	2.829	3.996	...
HE 0340−2612	03 42 27.80	−26 02 43.0	3.082	2.016	3.040	...
SDSS 0912+0547	09 12 10.35	+05 47 42.0	3.248	2.146	3.205	...
SDSS 0942+0422	09 42 02.04	+04 22 44.6	3.273	1.896	3.229	...
HE 0940−1050	09 42 53.40	−11 04 25.0	3.067	1.944	3.025	...
SDSS 0949+0355	09 49 32.27	+03 35 31.7	4.097	2.636	4.045	...
SDSS 1025+0452	10 25 09.64	+04 52 46.7	3.236	2.108	3.193	...
SDSS 1032+0541	10 32 49.88	+05 41 18.3	2.843	1.826	2.804	...
CTS 0291	10 33 59.90	−25 14 26.7	2.552	1.747	2.515	...
SDSS 1034+0358	10 34 56.31	+03 58 59.3	3.367	2.208	3.322	...
Q1100−264	11 03 25.60	−26 45 06.1	2.140	1.747	2.108	...
HS 1104+0452	11 07 08.40	+04 36 18.0	2.660	1.747	2.622	...
SDSS 1110+0244	11 10 08.61	+02 44 58.1	4.149	3.367	4.097	...
SDSS 1155+0530	11 55 38.60	+05 30 50.5	3.464	2.282	3.418	...
SDSS 1201+0116	12 01 44.36	+01 16 11.5	3.215	2.002	3.172	...
LB 1213+0922	12 15 39.60	+09 06 08.0	2.713	1.796	2.675	...
Q1224−0812	12 26 37.50	−08 29 29.0	2.142	1.747	2.110	...
SDSS 1249−0159	12 49 57.24	−01 59 28.8	3.662	2.406	3.614	...
SDSS 1307+0422	13 07 56.73	+04 22 15.5	3.026	1.821	2.985	...
LBQS 1334−0033	13 36 46.80	−00 48 54.2	2.809	1.829	2.770	...
SDSS 1336−0048	13 36 47.14	−00 48 57.2	2.806	1.796	2.767	...
SDSS 1339+0548	13 39 41.95	+05 48 22.1	2.969	1.969	2.928	...
HE 1347−2457	13 50 38.90	−25 12 17.0	2.599	1.749	2.562	...
Q1358+1154	14 00 39.10	+11 20 22.3	2.578	1.747	2.541	...
SDSS 1402+0146	14 02 48.07	+01 46 34.1	4.187	2.618	4.134	...
SDSS 1429−0145	14 29 03.03	−01 45 19.3	3.416	2.331	3.371	...
Q1456−1938	14 56 49.83	−19 38 52.0	3.163	1.879	3.120	...
SDSS 1503+0419	15 03 28.88	+04 19 49.0	3.666	3.126	3.618	...
SDSS 1521−0048	15 21 19.68	−00 48 18.6	2.935	2.178	2.895	...
SDSS 1558−0031	15 58 10.15	−00 31 20.0	2.831	1.784	2.792	...
Q1559+0853	16 02 22.60	+08 45 36.3	2.267	1.747	2.218	1.842, 2.251
SDSS 1621−0042	16 21 16.92	−00 42 50.8	3.704	2.142	3.656	...
Q1720+2501	17 22 52.90	+24 58 34.7	2.250	1.961	2.217	...
PKS 2000−330	20 03 24.10	−32 51 44.0	3.776	2.422	3.727	...
Q2044−1650	20 47 19.70	−16 39 05.8	1.939	1.747	1.909	...
Q2053−3546	20 53 44.60	−35 46 52.4	3.484	2.154	3.438	...
SDSS 2100−0641	21 00 25.03	−06 41 46.0	3.118	2.093	3.076	...
SDSS 2123−0050	21 23 29.46	−00 50 52.9	2.278	1.837	2.244	2.059
Q2126−158	21 29 12.20	−15 38 41.0	3.278	1.943	3.234	...
Q2147−0825	21 49 48.20	−08 11 16.2	2.127	1.879	2.095	...
SDSS 2159−0021	21 59 54.45	−00 21 50.1	1.963	1.797	1.932	...
HE 2156−4020	21 59 54.70	−40 05 50.0	2.530	1.747	2.494	...
HE 2215−6206	22 18 51.00	−61 50 43.0	3.317	1.720	3.273	...
Q2249−5037	22 52 44.00	−50 21 37.0	2.870	1.788	2.830	...
SDSS 2303−0939	23 03 01.45	−09 39 30.7	3.453	2.241	3.407	...
HE 2314−3405	23 16 43.20	−33 49 12.0	2.944	1.684	2.904	...
SDSS 2346−0016	23 46 25.67	−00 16 00.4	3.467	2.166	3.421	...
HE 2348−1444	23 51 29.80	−14 27 57.0	2.933	1.837	2.893	2.279
HE 2355−5457	23 58 33.40	−54 40 42.0	2.931	1.854	2.891	...

Note.—Units of right ascension are hours, minutes, and seconds, and units of declination are degrees, arcminutes, and arcseconds.

[a] These redshifts correspond to LLSs or DLAs that were known to exist along the QSO sight line prior to the higher resolution observations and also that inspired the observations.

TABLE 2
ESI Quasar Sample

Name	R.A. (J2000.0)	Decl. (J2000.0)	z_{em}	z_{start}	z_{end}	z_{mask}[a]
SDSS 0013+1358	00 13 28.21	+13 58 27.0	3.565	2.747	3.518	3.281
PX 0034+16	00 34 54.80	+16 39 20.0	4.290	3.031	4.207	4.260
SDSS 0058+0115	00 58 14.31	+01 15 30.3	2.535	2.373	2.499	...
SDSS 0127−00	01 27 00.70	−00 45 59.0	4.066	2.907	4.014	3.727
PSS 0134+3307	01 34 21.60	+33 07 56.0	4.525	3.154	4.469	3.761
SDSS 0139−0824	01 39 01.40	−08 24 43.0	3.008	2.373	2.967	2.677
SDSS 0142+0023	01 42 14.74	+00 23 24.0	3.363	2.356	3.303	3.347
SDSS 0225+0054	02 25 54.85	+00 54 51.0	2.963	2.331	2.922	2.714
SDSS 0316+0040	03 16 09.84	+00 40 43.2	2.907	2.331	2.866	...
BR J0426−2202	04 26 10.30	−22 02 17.0	4.328	3.039	4.274	2.980
FJ 0747+2739	07 47 11.10	+27 39 04.0	4.119	2.767	4.066	3.900, 3.423
PSS 0808+52	08 08 49.40	+52 15 15.0	4.440	3.155	4.385	3.113, 2.942
SDSS 0810+4603	08 10 54.90	+46 03 58.0	4.072	3.442	4.020	2.955
FJ 0812+32	08 12 40.70	+32 08 09.0	2.700	2.290	2.662	2.626
SDSS 0816+4823	08 16 18.99	+48 23 28.4	3.578	2.784	3.531	3.437
Q0821+31	08 21 07.60	+31 07 35.0	2.610	2.348	2.573	2.535
SDSS 0826+5152	08 26 38.59	+51 52 33.2	2.930	2.331	2.795	2.834, 2.862
SDSS 0844+5153	08 44 07.29	+51 53 11.0	3.193	2.373	3.150	2.775
SDSS 0912+5621	09 12 47.59	−00 47 17.4	2.967	2.373	2.851	2.890
Q0930+28	09 33 37.30	+28 45 32.0	3.436	2.529	3.391	3.246
PC 0953+47	09 56 25.20	+47 34 42.0	4.463	3.154	4.407	4.245, 3.889, 3.403
PSS 0957+33	09 57 44.50	+33 08 23.0	4.212	2.981	4.124	4.177, 3.280
SDSS 1004+0018	10 04 28.43	+00 18 25.6	3.042	2.422	3.001	2.540
BQ 1021+30	10 21 56.50	+30 01 41.0	3.119	2.290	3.076	2.949
CTQ 460	10 39 09.50	−23 13 26.0	3.134	2.290	3.091	2.778
HS 1132+22	11 35 08.10	+22 27 15.0	2.879	2.290	2.839	2.783
BRI 1144−07	11 46 35.60	−07 40 05.0	4.153	2.916	4.101	...
PSS 1159+13	11 59 06.48	+13 37 37.7	4.071	2.751	4.019	3.724
Q1209+09	12 11 34.90	+09 02 21.0	3.271	2.743	3.227	2.586
PSS 1248+31	12 48 20.20	+31 10 43.0	4.308	3.031	4.254	3.698
PSS 1253−02	12 53 36.30	−02 28 08.0	3.999	2.948	3.948	2.782
SDSS 1257−0111	12 57 59.22	−01 11 30.2	4.100	2.414	3.972	4.022
Q1337+11	13 40 02.60	+11 06 30.0	2.915	2.373	2.875	2.796
PSS 1432+39	14 32 24.80	+39 40 24.0	4.276	3.014	4.222	3.272
HS 1437+30	14 39 12.30	+29 54 49.0	2.991	2.290	2.950	2.874
SDSS 1447+5824	14 47 52.47	+58 24 20.2	2.971	2.389	2.930	2.818
SDSS 1453+0023	14 53 29.53	+00 23 57.5	2.531	2.373	2.495	2.444
SDSS 1610+4724	16 10 09.42	+47 24 44.5	3.201	2.373	3.158	2.508
PSS 1723+2243	17 23 23.20	+22 43 58.0	4.515	3.006	4.459	3.695
SDSS 2036−0553	20 36 42.29	−05 52 60.0	2.575	2.414	2.538	2.280
FJ 2129+00	21 29 16.60	+00 37 56.6	2.954	2.290	2.913	2.735
SDSS 2151−0707	21 51 17.00	−07 07 53.0	2.516	2.406	2.480	2.327
SDSS 2222−0946	22 22 56.11	−09 46 36.2	2.882	2.784	2.842	2.354
Q2223+20	22 25 36.90	+20 40 15.0	3.574	2.344	3.527	3.119
SDSS 2238+0016	22 38 43.56	+00 16 47.0	3.425	2.455	3.321	3.365
PSS 2241+1352	22 41 47.70	+13 52 03.0	4.441	3.483	4.385	4.283
SDSS 2315+1456	23 15 43.56	+14 56 06.0	3.370	2.373	3.326	3.273
PSS 2323+2758	23 23 40.90	+27 57 60.0	4.131	2.907	4.078	3.684
FJ 2334−09	23 34 46.40	−09 08 12.0	3.326	2.307	3.282	3.057
SDSS 2343+1410	23 43 52.62	+14 10 14.0	2.907	2.373	2.867	2.677
Q2342+34	23 44 51.20	+34 33 49.0	3.030	2.735	2.989	2.908
SDSS 2350−00	23 50 57.87	−00 52 09.9	3.010	2.866	2.969	2.615

Note.—Units of right ascension are hours, minutes, and seconds, and units of declination are degrees, arcminutes, and arcseconds.
[a] These redshifts correspond to LLSs or DLAs that were known to exist along the QSO sight line prior to the higher resolution observations and also that inspired the observations.

and we wish to avoid biasing the sample (because these systems frequently motivated the observations). We mask out regions 1500 km s^{-1} on either side of the DLA redshifts from the redshift path (corresponding to ≈15 comoving Mpc h^{-1} at $z = 3$) to prevent SLLSs clustering with DLAs from biasing the sample. In this fashion we construct a sensitivity function $g_i(z)$ that has unit value at redshifts where SLLSs could be detected and zero otherwise. The combined redshift path of our sample is $\Delta z = 124.4$.

The H I frequency distribution function $f_{\rm H\,I}(N, X)$ for the SLLS describes the number of SLLSs in a range of column densities $(N, N + dN)$ and a range of absorption distances $(X, X + dX)$,

$$f_{\rm H\,I}(N, X)\, dN\, dX, \qquad (1)$$

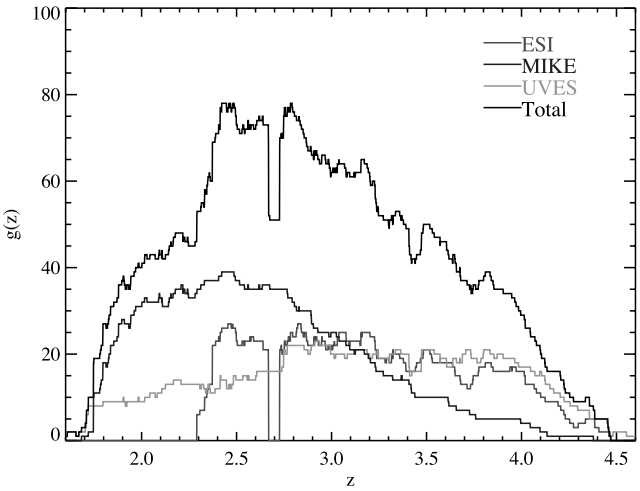

FIG. 1.—Redshift sensitivity function $g(z)$ for the samples. The sharp feature at $z \simeq 2.7$ is caused by a gap in the ESI data. The upper curve represents the full sample $g(z)$ subject to the added constraint that it apply to the data where an SLLS with $N_{\rm H\,I} > 19.3$ cm^{-2} could be found, with the other curves representing the $g(z)$ for the MIKE, ESI, and UVES data samples that comprise the full sample. [*See the electronic edition of the Journal for a color version of this figure.*]

where the absorption distance (Bahcall & Peebles 1969) is given by

$$\Delta X = \int dX = \int \frac{H_0}{H(z)}(1+z)^2\, dz. \qquad (2)$$

By considering dX instead of dz, $f_{\rm H\,I}(N, X)$ is defined over a constant, comoving path length, but we have introduced our assumed cosmology into the analysis (e.g., Lanzetta 1993). The cosmological term in $f_{\rm H\,I}(N, X)$ is still relatively obscure but can be made less so when we consider that for $z > 2$, $dX/dz \approx [(1+z)/\Omega_m]^{1/2}$ for a standard ΛCDM model. By way of example, consider a sight line with $\Delta z = 1$ path length at the average redshift for our survey $\bar{z} = 3.1$ corresponding to $\Delta X \approx 3.7$.

To characterize the survey size, we construct the total redshift sensitivity function, $g(z) = \Sigma_i g_i(z)$. Figure 1 shows the $g(z)$ curves for the MIKE, ESI, and UVES samples and the combined $g(z)$ for all three samples. We find that the total sample presented here increases $g(z)$ by factors of 2–8 over the redshift range $2 \leq z \leq 4$ when compared to the previous survey of Péroux et al. (2005) when we consider the column density range 19.3 cm$^{-2} \leq \log N_{\rm H\,I} \leq$ 20.2 cm^{-2}. In Figure 1, there is a sharp feature in $g(z)$ at a redshift of $z \simeq 2.7$. This feature is due to a gap in the ESI data at $\lambda \simeq$ 4500 Å that appears in every ESI spectrum in the sample. At the redshifts surveyed, the resolution of the data is sufficiently high that sky lines do not affect our ability to detect LLSs in the data.

3. $N_{\rm H\,I}$ ANALYSIS

With the survey size defined, we now turn to the SLLSs in the survey and discuss the measurement of the $N_{\rm H\,I}$ for the SLLSs and an estimate of the completeness of the sample.

3.1. *Identifying SLLSs and Measuring* $N_{\rm H\,I}$

To identify the SLLSs in our survey, every spectrum from the ESI and MIKE samples was visually inspected for strong absorption in H I Lyα. When a candidate SLLS absorber is identified, we first assign a local continuum level to regions approximately 2000 km s^{-1} on either side of the absorption. We do not first continuum normalize the data, opting instead to model the absorption and continuum simultaneously. This is done because the damping wings of the Lyα profile may depress the continuum for several tens of angstroms. It is also necessary to vary the continuum level along with a model to estimate the errors on the $N_{\rm H\,I}$ values. When the absorption occurs near the QSO emission line features and/or when the redshift of the absorption is high, the assignment of the continuum level is often the dominant source of error. In this work, we assign a *minimum* value of the error on the $\log N_{\rm H\,I}$ to be 0.05 dex from continuum level errors alone.

Next, we compared a Voigt profile with $\log N_{\rm H\,I} = 19.0$ cm^{-2} at the center of the absorption to determine if it was consistent with at least this amount of atomic hydrogen gas. If metal-line transitions were identified, we use the redshift of the metals to more accurately assign a redshift for the gas. We do not, however, require that metal-line absorption be present because this would introduce an undesirable bias. For most of the absorption systems in our sample, the data cover a wide variety of metal-line transitions for each absorber. Common transitions include those of C II, C IV, O I, Si II, Si IV, Al II, and Fe II. In the cases where both low- and high-ionization metal-line transitions are present, we choose to use the redshift given by the low-ion absorption because these ions more likely trace the atomic hydrogen gas. Finally, for those absorbers meeting our minimum $N_{\rm H\,I}$ condition, we fit the absorption by stepping through values of $N_{\rm H\,I}$ until the absorption is well modeled. The Lyα line profile and continuum level were modeled using custom software (the `x_fitdla` tool within the XIDL package[10]). In the cases when two or more SLLSs occur within $\delta v \leq 300$ km s^{-1} of each other, the *total* $N_{\rm H\,I}$ is reported instead of individual $N_{\rm H\,I}$ measurements. This is because the individual $N_{\rm H\,I}$ measurements are highly degenerate and because the gas may be physically bound to a single virialized halo.

For each absorber, a number of effects contribute to the error in the $N_{\rm H\,I}$ value. As mentioned above, we believe that errors in the continuum level contribute at least 0.05 dex to the error. The continuum level error tends to increase with redshift because the amount of absorption from Lyα forest increases and one is less certain to identify regions free of absorption. The increase in Lyα forest lines also affects the $N_{\rm H\,I}$ measurement in the damping wings and line core regions of the Lyα line because of enhanced line blending. Redshift uncertainties were only a minor source of error for each absorber, since nearly every absorption system showed at least one metal-line transition. Finally, the Poisson noise of the data adds additional uncertainty to the fitted value.

In Figures 2 and 3 we show the profile fits and the $\pm 1\ \sigma$ fits for each LLS in our sample. The values for the z, $N_{\rm H\,I}$, and $\sigma(N_{\rm H\,I})$ are given in Tables 3 and 4. The LLSs listed in these tables do not represent every LLS present in our data. In a number of cases, we removed an SLLS from the sample because the QSO was specifically targeted to study this SLLS. For those SLLSs removed, we also remove 1500 km s^{-1} of path length on either side of the SLLS in the same manner as for the DLA. In total, we have a homogeneous sample of 47 SLLSs, of which 17 come from the ESI sample and 30 come from the MIKE sample. Including the UVES sample, there are now a total of 78 SLLSs. In Figure 4 we show a histogram of the $N_{\rm H\,I}$ values for the individual and complete samples.

3.2. *Completeness*

To gauge the completeness of our $N_{\rm H\,I}$ analysis, we performed a number of tests. Our primary completeness concern is with the detection efficiency at the low H I column density limit

[10] See http://www.ucolick.org/~xavier/IDL/.

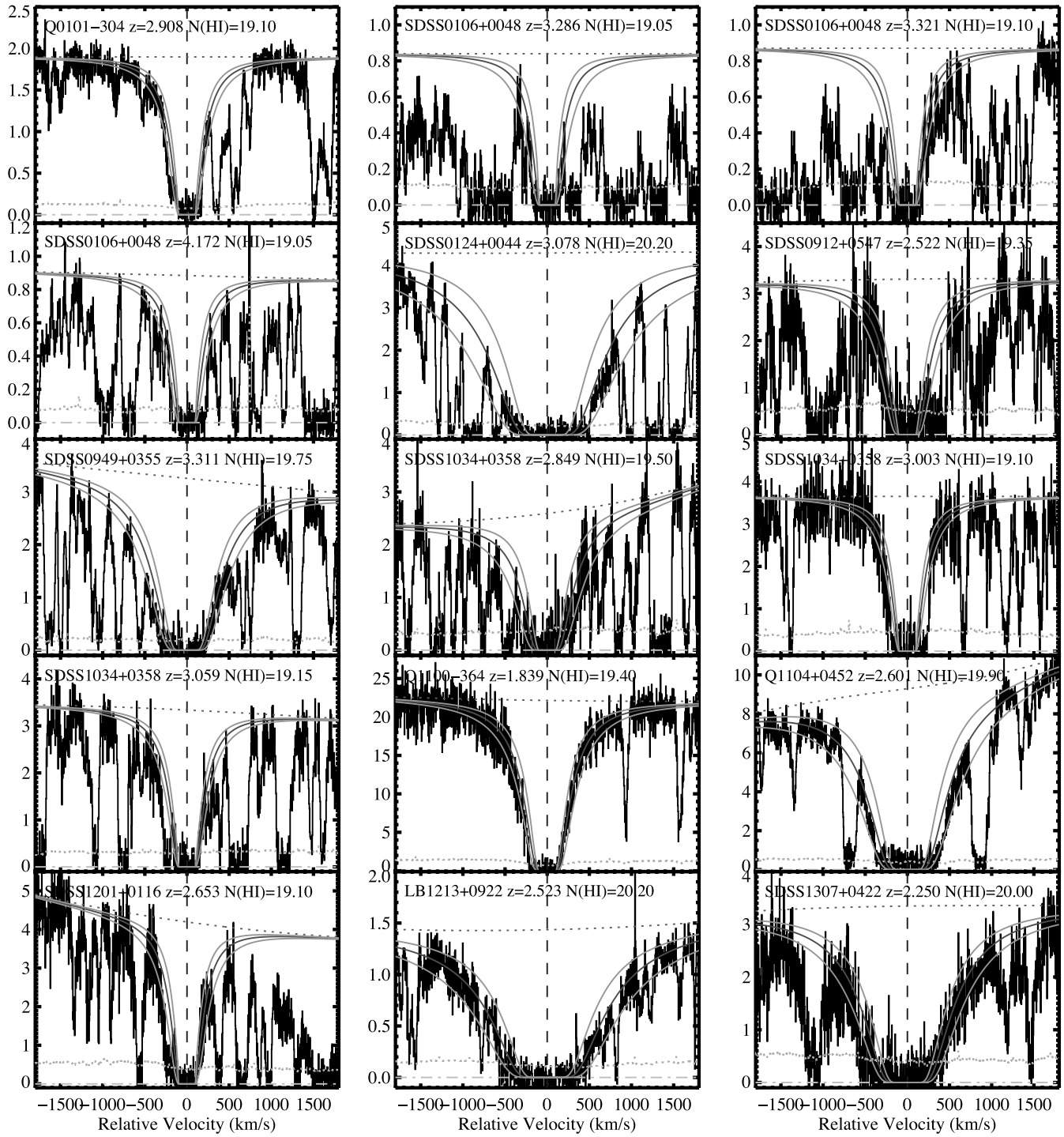

FIG. 2.—H I Lyα transitions for the SLLSs in the MIKE sample. The velocity zero point is determined from low-ionization metal lines whenever possible. Overlaid are the single-component Voigt profile models for the absorption along with the $\pm 1\ \sigma$ error estimates on the $N_{\rm H\,I}$. The horizontal dashed line represents the local continuum level. The vertical dashed line highlights the velocity zero point. For each absorber, the QSO name, absorption redshift, and $N_{\rm H\,I}$ estimate are listed at the top of each panel. In the case of blended SLLSs where the individual Lyα lines are separated by more than 300 km s^{-1}, we show the individual fits (e.g., the SLLS in PKS 2000−330). [*See the electronic edition of the Journal for a color version of this figure.*]

of the ESI sample, where the data have lower spectral resolution. At lower resolution, the effects of line blending and continuum level placement tend to wash out the damping wings of $\log N_{\rm H\,I} \simeq 19.0$ Lyα lines. As the column density increases, the equivalent width of the Lyα line also increases and one generally derives a more reliable $N_{\rm H\,I}$ measurement. Because the MIKE and UVES samples are of higher resolution, the effect at lower column densities is minimized. After experimenting with mock ESI spectra (see below), we chose to limit the ESI analysis to those absorbers with $19.3\ {\rm cm}^{-2} \leq \log N_{\rm H\,I} \leq 20.3\ {\rm cm}^{-2}$. For the MIKE sample, we consider the same range of column densities as in the UVES sample, $19.0\ {\rm cm}^{-2} \leq \log N_{\rm H\,I} \leq 20.3\ {\rm cm}^{-2}$. Our tests indicate that we have detected all SLLSs in these ranges in $N_{\rm H\,I}$ at a 99% level of completeness.

To verify that the lower bound of $\log N_{\rm H\,I} = 19.3\ {\rm cm}^{-2}$ is appropriate for the ESI sample, we randomly placed mock LLSs

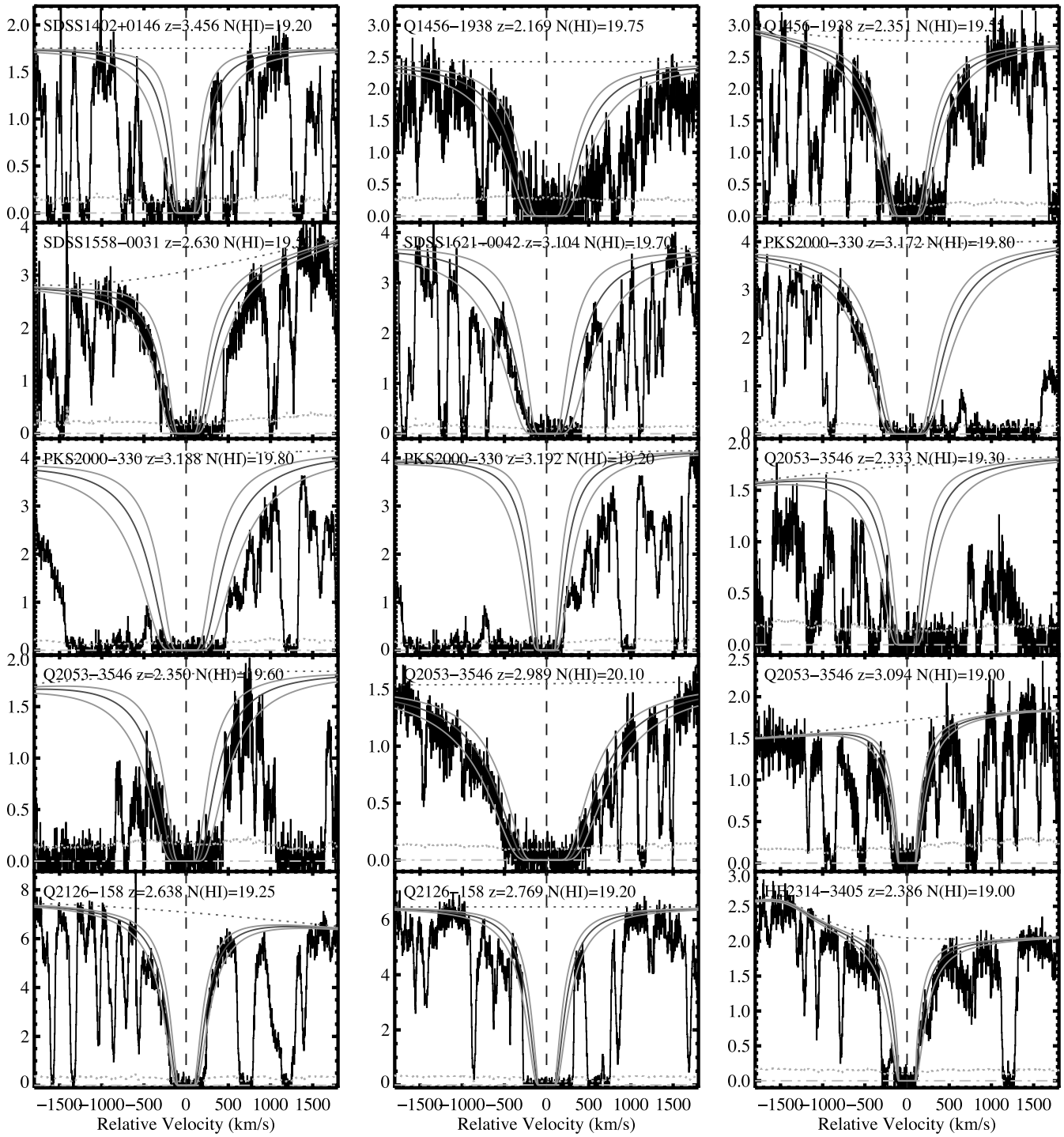

FIG. 2—*Continued*

onto 50 of the ESI spectra. The column densities of these LLSs were chosen at random to lie in the range 18.0 $\mathrm{cm}^{-2} \leq \log N_{\mathrm{H\,I}} \leq$ 20.5 cm^{-2}. In all cases, SLLSs with $\log N_{\mathrm{H\,I}} \geq 19.3$ cm^{-2} were identified. Furthermore, the column density fits to these SLLSs were within the 2 σ error estimates in all cases but 1 out of 50. We have also used simulated LLSs to address the issue that blending of multiple LLSs with $\log N_{\mathrm{H\,I}} \leq 19.3$ cm^{-2} could appear as a single absorber with $\log N_{\mathrm{H\,I}} \geq 19.3$ cm^{-2} in the ESI sample. As before, we placed mock LLSs on ESI spectra, but in pairs with a random velocity separation δv subject to the constraint $\delta v \leq 300$ km s^{-1}. The blended, mock LLS absorption was then fitted with a single absorption profile, and the $N_{\mathrm{H\,I}}$ compared to the sum of the individual component $N_{\mathrm{H\,I}}$ values. We find that a pair of LLSs with $\log N_{\mathrm{H\,I}} \leq 18.8$ cm^{-2} or less cannot blend in a manner so as to be fitted as an SLLS with $\log N_{\mathrm{H\,I}} \geq 19.3$ cm^{-2}. However, a blend of an SLLS with $\log N_{\mathrm{H\,I}} \geq 19.3$ cm^{-2} with an LLS with $\log N_{\mathrm{H\,I}} \sim 19.1$ cm^{-2} generally leads to a systematic overestimate of $N_{\mathrm{H\,I}}$. Similarly, a blend of LLSs with $\log N_{\mathrm{H\,I}} =$ 19.1 cm^{-2} and $\log N_{\mathrm{H\,I}} = 18.8$ cm^{-2} may mimic an SLLS with $\log N_{\mathrm{H\,I}} = 19.3$ cm^{-2}. In essence, this effect leads to a Malmquist bias for the sample at low $N_{\mathrm{H\,I}}$ value. It is not generally possible to directly explore these final two issues without good knowledge

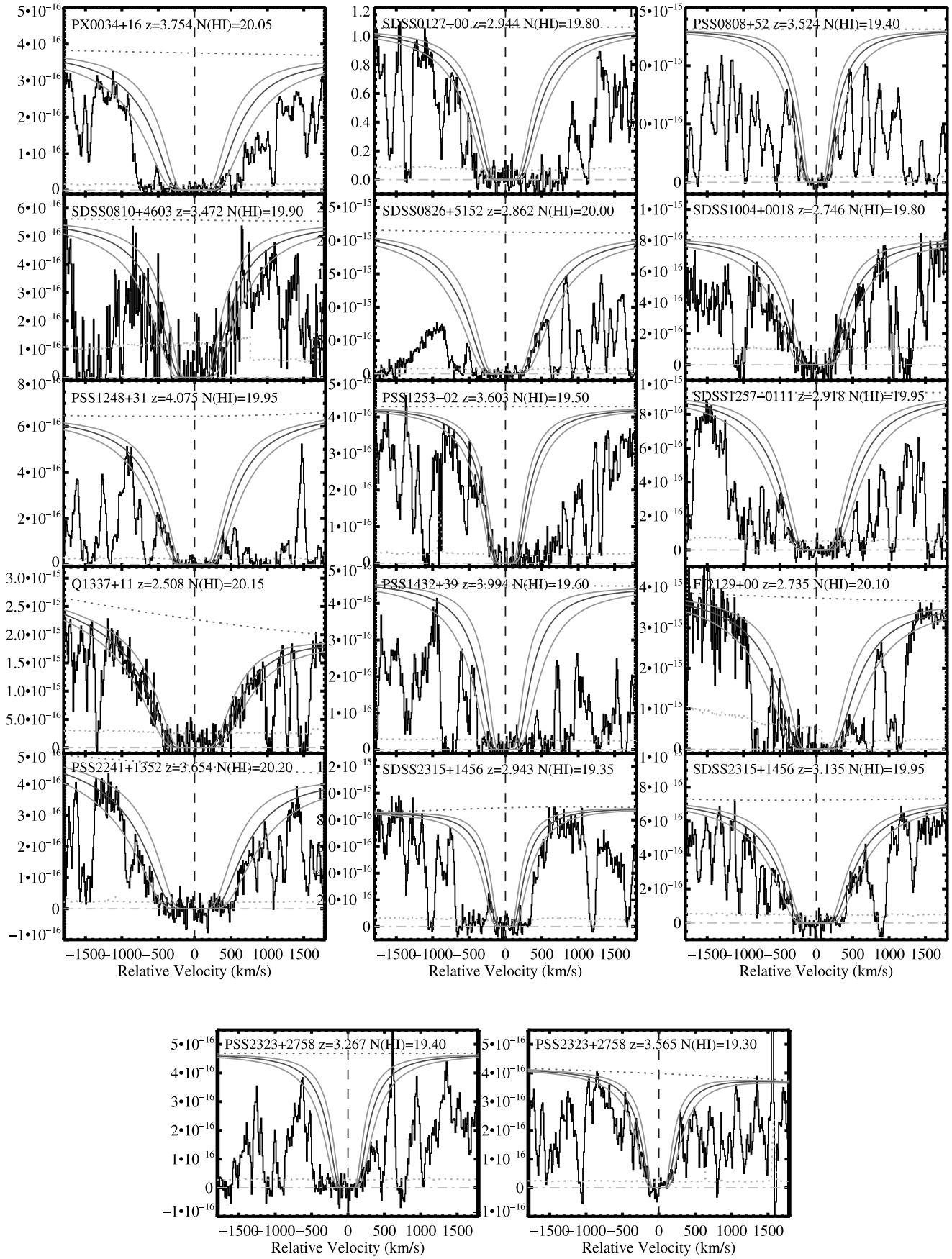

FIG. 3.—Same as for Fig. 2, but for the SLLSs in the ESI sample. [*See the electronic edition of the Journal for a color version of this figure.*]

TABLE 3
LLSs from the MIKE Sample

Name	z_{abs}	$\log N_{H\,I}$	$\sigma(N_{H\,I})$
Q0101−304	2.908	19.10	0.15
SDSS 0106+0048	3.286	19.05	0.25
SDSS 0106+0048	3.321	19.10	0.20
SDSS 0106+0048	4.172	19.05	0.20
SDSS 0124+0044	3.078	20.20	0.20
SDSS 0912+0547	2.522	19.35	0.20
SDSS 0949+0355	3.311	19.75	0.15
SDSS 1034+0358	2.849	19.50	0.25
SDSS 1034+0358	3.059	19.15	0.15
SDSS 1034+0358	3.003	19.10	0.15
Q1100−264	1.839	19.40	0.15
HS 1104+0452	2.601	19.90	0.20
LB 1213+0922	2.523	20.20	0.20
SDSS 1307+0422	2.250	20.00	0.15
SDSS 1402+0146	3.456	19.20	0.30
Q1456−1938	2.351	19.55	0.15
Q1456−1938	2.169	19.75	0.20
SDSS 1558−0031	2.630	19.50	0.20
SDSS 1621−0042	3.104	19.70	0.20
PKS 2000−330	3.188	19.80	0.25
PKS 2000−330	3.172	19.80	0.15
PKS 2000−330	3.192	19.20	0.25
Q2053−3546	2.350	19.60	0.25
Q2053−3546	2.989	20.10	0.15
Q2053−3546	3.094	19.00	0.15
Q2053−3546	2.333	19.30	0.25
Q2126−158	2.638	19.25	0.15
Q2126−158	2.769	19.20	0.15
HE 2314−3405	2.386	19.00	0.20

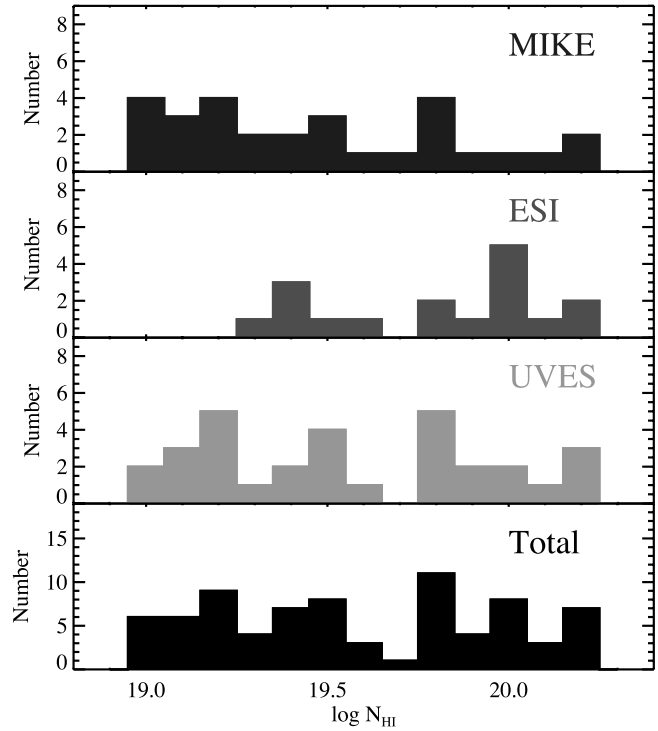

Fig. 4.—Histograms showing the number of systems detected as a function of $\log N_{H\,I}$ for the various samples. The top two panels represent the MIKE and ESI data, which are presented for the first time in this paper. The third panel shows the data from Péroux et al. (2005). The bottom panel shows the full $N_{H\,I}$ histogram when we combine the three data sets. [*See the electronic edition of the Journal for a color version of this figure.*]

of the incidence frequency, clustering properties, and column density distribution of the LLS. Nevertheless, we have some constraints from both the MIKE and UVES samples. Because these samples are of higher resolution, we can often distinguish blended absorption of LLSs from a single LLS. Moreover, if two LLSs are blended, their metal lines should give some clues that there is blending, provided that both LLSs have sufficient metallicity. To the extent that we can currently distinguish between blended and unblended LLSs, we do not believe that the effect of blended LLSs strongly affects our measurements of the $N_{H\,I}$, but we caution that a larger sample than the one presented here is required to accurately address this issue.

TABLE 4
LLSs from the ESI Sample

Name	z_{abs}	$\log N_{H\,I}$	$\sigma(N_{H\,I})$
PX 0034+16	3.754	20.05	0.20
SDSS 0127−00	2.944	19.80	0.15
PSS 0808+52	3.524	19.40	0.20
SDSS 0810+4603	3.472	19.90	0.20
SDSS 0826+5152	2.862	20.00	0.15
SDSS 1004+0018	2.746	19.80	0.20
PSS 1248+31	4.075	19.95	0.15
PSS 1253−02	3.603	19.50	0.15
SDSS 1257−0111	2.918	19.95	0.15
Q1337+11	2.508	20.15	0.15
PSS 1432+39	3.994	19.60	0.25
FJ 2129+00	2.735	20.10	0.20
PSS 2241+1352	3.654	20.20	0.20
SDSS 2315+1456	3.135	19.95	0.15
SDSS 2315+1456	2.943	19.35	0.20
PSS 2323+2758	3.267	19.40	0.20
PSS 2323+2758	3.565	19.30	0.20

4. RESULTS AND DISCUSSION

In this section we discuss a number of results related to the H I frequency distribution of the SLLSs. For the majority of the section, we consider two $N_{H\,I}$ groups driven by the completeness limits of the spectra: (1) $10^{19.0}$ cm$^{-2} \leq N_{H\,I} \leq 10^{20.3}$ cm^{-2}, which does not include the ESI sample; and (2) $10^{19.3}$ cm$^{-2} \leq N_{H\,I} \leq 10^{20.3}$ cm^{-2}, which includes all of the samples. The groups cover an integrated absorption path length of $\Delta X^{19.0} = 329.1$ and $\Delta X^{19.3} = 467.7$, respectively. We maintain this division, as opposed to combining the low-$N_{H\,I}$ results from the echelle data with the $N_{H\,I} \geq 10^{19.3}$ cm^{-2} analysis, for the following reasons: First, the redshift distribution of the ESI survey (Fig. 1) is significantly higher than that of the UVES data and especially the MIKE sample. If there is redshift evolution in $f_{H\,I}(N, X)$, then it would be erroneous to mix the two groups. Indeed, PHW05 find significant evolution in the normalization of $f_{H\,I}(N, X)$ for the DLAs, and one may expect similar evolution in the SLLS population. Second, the division allows us to investigate systematic errors between the various surveys, including the UVES analysis. Finally, we find it instructively valuable to consider these two $N_{H\,I}$ groups separately when focusing on the behavior of $f_{H\,I}(N, X)$ near $N_{H\,I} = 10^{19}$ cm^{-2}.

4.1. *Power-Law Fits to the $f_{H\,I}(N, X)$ Distribution of the SLLS*

In Figures 5 and 6 we show the binned evaluation of $f_{H\,I}(N, X)$ for each of the data sets and their combined results. The results

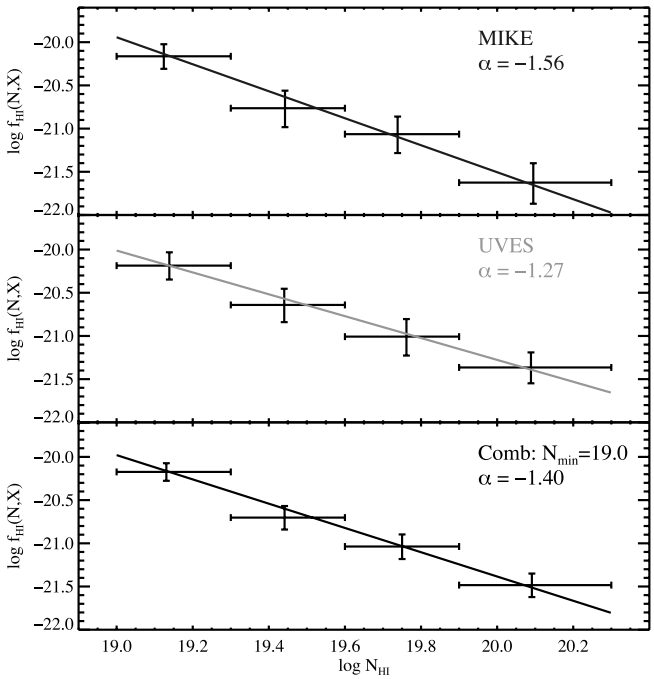

FIG. 5.—Values for the H I frequency distribution for the SLLSs with 19.0 $cm^{-2} \leq \log N_{H\,I} \leq 20.3$ cm^{-2}. Shown separately are the MIKE data presented first here, the UVES sample of Péroux et al. (2003a, 2005), and the two samples combined. The four bins span equal size $\Delta \log N_{H\,I} = 0.3$ except for the last bin, which has $\Delta \log N_{H\,I} = 0.4$. Also shown is the result of a maximum likelihood analysis on the unbinned data for a power-law model of $f_{H\,I}(N, X)$. The power-law index α is given for each sample. [*See the electronic edition of the Journal for a color version of this figure.*]

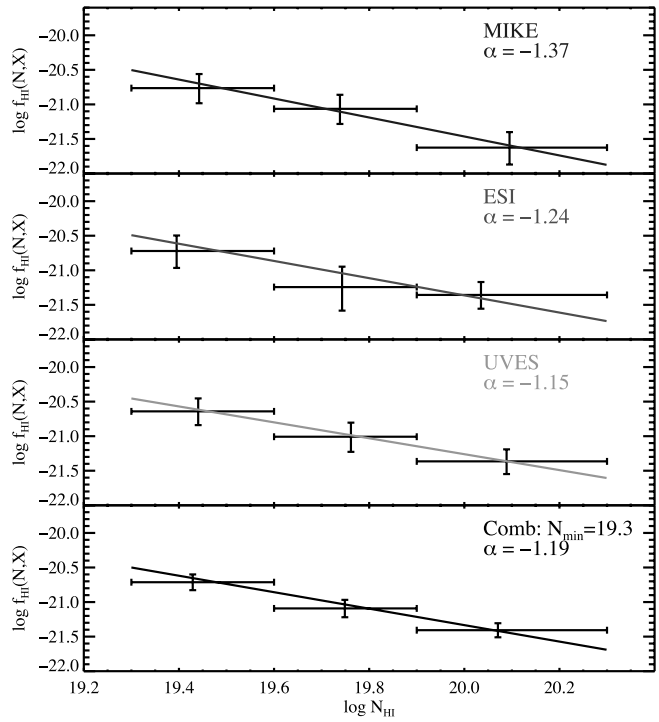

FIG. 6.—Same as for Fig. 5, but with the inclusion of the ESI data, and with the range 19.0 $cm^{-2} \leq \log N_{H\,I} \leq 20.3$ cm^{-2}, over 3 bins equal in size to the 3 highest H I column density bins in Fig. 5. Also shown is the result of a maximum likelihood analysis on the unbinned data for a power-law model of $f_{H\,I}(N, X)$. The power-law index α is given for each sample. [*See the electronic edition of the Journal for a color version of this figure.*]

are summarized in Table 5. It is evident from the figures that the $f_{H\,I}(N, X)$ distributions can be reasonably modeled by a power law over the SLLS regime:

$$f_{H\,I}(N, X) = k_1 N^{\alpha}. \tag{3}$$

We have performed a maximum likelihood analysis on the unbinned $N_{H\,I}$ distribution to constrain α and set the normalization of $f_{H\,I}(N, X)$. We find $\alpha_{190} = -1.40^{+0.15}_{-0.16}$ and $\alpha_{193} = -1.19^{+0.20}_{-0.21}$ for the combined results of the two groups. Note that the reported errors do not include covariance terms. The results for the individual data samples are all consistent (within 2 σ) with the combined results and one another (Table 5).

One notes that the power law is shallower for the $N_{H\,I}^{19.3}$ sample than the $N_{H\,I}^{19.0}$ sample. Although the effect is not statistically significant, we do find that the trend is apparent in the independent MIKE and UVES samples. These results suggest that the $f_{H\,I}(N, X)$ distribution is steepening at $N_{H\,I} < 10^{19.3}$ cm^{-2}. We return to this point in § 4.4.

4.2. *Redshift Evolution*

Over the redshift interval $z = 2.2$–3.5, PHW05 found that the shape of $f_{H\,I}(N, X)$ for DLAs is roughly constant but that the normalization (parameterized by the zeroth moment, ℓ_{DLA}) increases by a factor of approximately 2. Similarly, studies of the Lyα forest indicate $\ell(z)^{Ly\alpha} \propto (1+z)^{2.6}$ (Cristiani et al. 1995) at $z \approx 3$, implying $\ell(X)^{Ly\alpha} \propto (1+z)^{2.1}$. One may expect, therefore, that $\ell_{SLLS}(X)$ will also increase with redshift over this redshift interval.

In Figure 7 we show the results for $f_{H\,I}(N, X)$ in the two $N_{H\,I}$ groups, but broken into the redshift regions above (*thin line*) and below (*thick line*) $z = 3$. A visual inspection of Figure 7 reveals little explicit difference in the shape of $f_{H\,I}(N, X)$ in the two redshift regimes. More formally, a K-S test for the two groups returns probabilities of $P_{190} = 0.189$ and $P_{193} = 0.809$ that the two redshift samples are drawn from the same parent population. Therefore, we contend that there is no large redshift evolution in the shape of $f_{H\,I}(N, X)$ for the SLLS over the redshifts considered here.

Granted that the shape of $f_{H\,I}(N, X)$ for the SLLS is not steeply evolving, we can examine redshift variations in the normalization by examining the zeroth moment

$$\ell_{SLLS}(X) = \int_{N_{SLLS}}^{10^{20.3}} f_{H\,I}(N, X)\, dN, \tag{4}$$

with $N_{SLLS} = 10^{19.0}$ or $10^{19.3}$ cm^{-2}. We calculate $\ell_{SLLS}(X)_{(190)} = 0.134^{+0.032}_{-0.026}$ and $\ell_{SLLS}(X)_{(193)} = 0.110^{+0.026}_{-0.021}$ for $z < 3$ and $\ell_{SLLS}(X)_{(190)} = 0.254^{+0.050}_{-0.042}$ and $\ell_{SLLS}(X)_{(193)} = 0.126^{+0.028}_{-0.023}$ for $z > 3$. As is evident from Figure 7 (i.e., focus on the values for the lowest $N_{H\,I}$ bins), there is no significant redshift evolution in $\ell_{SLLS}(X)$ for the $N_{H\,I} = 10^{19.3}$ cm^{-2} sample. There is, however, an indication of increasing $\ell_{SLLS}(X)$ with increasing redshift for the $N_{H\,I} = 10^{19.0}$ cm^{-2} sample. This result is driven by the lowest $N_{H\,I}$ bin, which we caution is the most sensitive to the effects of line blending and that such effects are heightened at higher redshift. In summary, there is only tentative evidence for redshift evolution in $\ell_{SLLS}(X)$. As noted above, this contradicts the apparent evolution in $\ell(X)$ for the DLA population and the Lyα forest. If confirmed by future studies, perhaps modest evolution in the SLLS population suggests the competing effects of the decrease in the

TABLE 5

$f_{\rm H\,I}(N, X)$ Summary

Sample	ΔX	$\bar{z}$	$m_{\rm SLLS}$	$\log f_{\rm H\,I}(N, X)$ $N_{\rm H\,I}\epsilon[19.0, 19.3)$	$N_{\rm H\,I}\epsilon[19.3, 19.6)$	$N_{\rm H\,I}\epsilon[19.6, 19.9)$	$N_{\rm H\,I}\epsilon[19.9, 20.3)$	$\ell_{\rm SLLS}(X)$	$\log k_1$	α_1
ESI	132.5	3.34	15	...	$-20.72^{+0.22}_{-0.24}$	$-21.24^{+0.30}_{-0.34}$	$-21.36^{+0.19}_{-0.20}$	$0.113^{+0.037}_{-0.029}$	$3.527^{+0.124}_{-0.128}$	$-1.244^{+0.390}_{-0.404}$
MIKE	175.6	2.85	29	$-20.16^{+0.14}_{-0.15}$	$-20.76^{+0.20}_{-0.22}$	$-21.06^{+0.20}_{-0.22}$	$-21.63^{+0.22}_{-0.24}$	$0.165^{+0.037}_{-0.030}$	$9.735^{+0.087}_{-0.088}$	$-1.562^{+0.224}_{-0.240}$
UVES	154.2	3.33	31	$-20.19^{+0.15}_{-0.16}$	$-20.64^{+0.19}_{-0.20}$	$-21.01^{+0.20}_{-0.22}$	$-21.36^{+0.17}_{-0.18}$	$0.201^{+0.043}_{-0.036}$	$4.033^{+0.084}_{-0.085}$	$-1.265^{+0.209}_{-0.216}$
ALL-19.3	467.7	3.08	55	...	$-20.71^{+0.11}_{-0.12}$	$-21.09^{+0.12}_{-0.13}$	$-21.41^{+0.10}_{-0.10}$	$0.118^{+0.018}_{-0.016}$	$2.486^{+0.062}_{-0.062}$	$-1.191^{+0.203}_{-0.206}$
ALL-19.0	329.8	3.10	60	$-20.17^{+0.10}_{-0.10}$	$-20.70^{+0.13}_{-0.14}$	$-21.04^{+0.14}_{-0.15}$	$-21.48^{+0.13}_{-0.14}$	$0.182^{+0.027}_{-0.023}$	$6.716^{+0.059}_{-0.059}$	$-1.405^{+0.153}_{-0.158}$

mean density of the universe and a decrease in the intensity of the extragalactic UV background radiation field.

4.3. *Is $f_{\rm H\,I}(N, X)$ for the SLLS Flatter than the DLA?*

There is a significant mismatch in power-law exponents for the Lyα forest ($\alpha_{\rm Ly\alpha} = -1.5$) and the DLA ($\alpha_{\rm DLA} \approx -2$) at $z \approx 3$. This difference predicts that the shape of $f_{\rm H\,I}(N, X)$ changes appreciably between these two column densities, i.e., the $f_{\rm H\,I}(N, X)$ distribution of SLLSs is flatter than that of the DLA.

The simplest test of this prediction is to measure the power-law index of $f_{\rm H\,I}(N, X)$ in the SLLS regime and compare against its slope near $N_{\rm H\,I} = 10^{20.3}$ cm^{-2}. Both the gamma function and double power-law fits to $f_{\rm H\,I}(N, X)$ for the SDSS DLA sample indicate $\alpha_{\rm DLA} = -1.9 \pm 0.1$ at $N_{\rm H\,I} < 10^{21}$ cm^{-2} (PHW05). We compare these values with $\alpha_{\rm SLLS} = -1.19 \pm 0.21$ for $\log N^{\rm lim}_{\rm H\,I} = 19.3$ cm^{-2} and $\alpha_{\rm SLLS} = -1.40 \pm 0.15$ for $\log N^{\rm lim}_{\rm H\,I} = 19.0$ cm^{-2}. The statistical difference in the power-law slope is greater than 2 σ significance but not a full 3 σ result, in terms of the exponents alone.

Figure 8 shows the $f_{\rm H\,I}(N, X)$ distributions for the SLLS and SDSS DLA to a column density of $\log N_{\rm H\,I} = 21.5$ cm^{-2}. As before, we show the results for the different SLLS $N_{\rm H\,I}$ groups separately. Overplotted on the data are the SLLS single power-law fit and the low column density end of the double power law for the SDSS DLA (PHW05). It is apparent that a simple extrapolation of the SDSS DLA fit significantly overpredicts the frequency of the SLLS, especially at $\log N_{\rm H\,I} < 19.7$ cm^{-2}. We contend, therefore, that the $f_{\rm H\,I}(N, X)$ flattens in slope around the $N_{\rm H\,I}$ corresponding to the canonical definition for the DLA, $\log N_{\rm H\,I} = 20.3$ cm^{-2}. Zheng & Miralda-Escudé (2002) predicted a flattening in $f_{\rm H\,I}(N, X)$ based on photoionization and self-shielding models of isothermal gas profiles in dark matter halos. Although their analysis examined individual halos at a given mass, Z. Zheng (2006, private communication) has convolved their results with a Sheth-Tormen halo mass function (Sheth & Tormen 1999) and predicts that $f_{\rm H\,I}(N, X)$ should flatten at $N_{\rm H\,I} \approx 10^{20}$ cm^{-2}, consistent with our results.

There are a few cautionary remarks to make regarding Figure 8. First, the shapes of the selection functions $g(z)$ for the SLLS and DLA samples do not exactly match because the SLLS database includes a somewhat higher fraction of $z > 3$ quasars and thus a

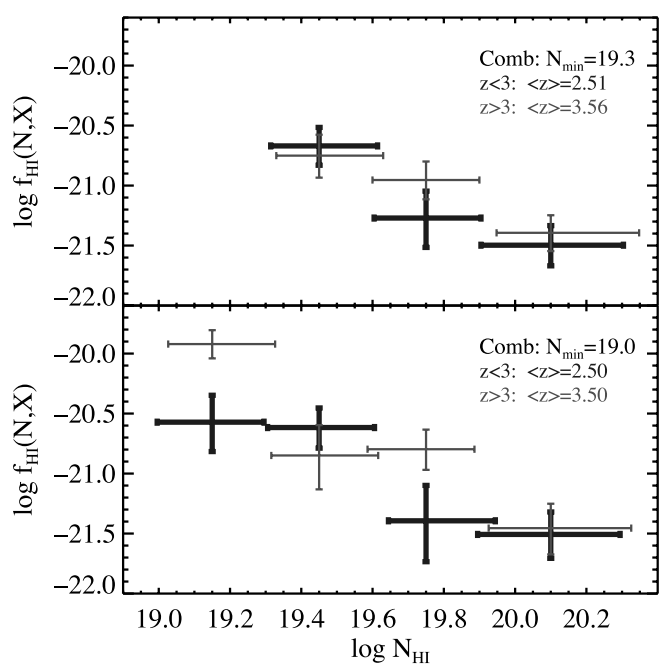

Fig. 7.—Values for the H I frequency distribution for the SLLSs separated into two redshift samples, with the thin symbols corresponding to $z < 3$ and the thick symbols corresponding to $z > 3$. The top panel shows the ESI+MIKE+UVES sample and the bottom panel the MIKE+UVES sample. The lack of significant change in shape of $f_{\rm H\,I}(N, X)$ for the two redshift bins indicates a lack of strong evolution with redshift in $f_{\rm H\,I}(N, X)$. [*See the electronic edition of the Journal for a color version of this figure.*]

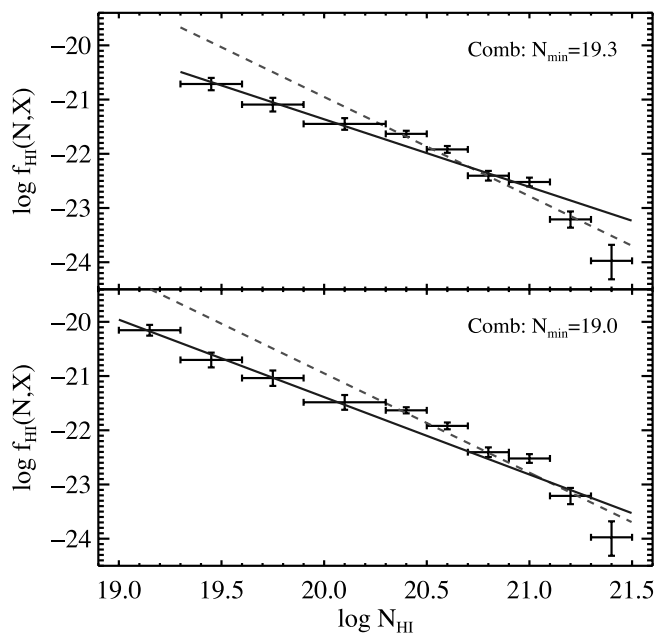

Fig. 8.—Values for the H I frequency distribution for both the SLLS and the DLA sample of PHW05. Overplotted are the results for the single power law for the SLLSs from this work (*dot-dashed line*; power-law index $\alpha = -1.19$ and -1.40 for the top and bottom panels, respectively), and the low column density end of the double power-law fits to $f_{\rm H\,I}(N, X)$ for the DLAs from PHW05 (*dashed line*; power-law index $\alpha = -2.0$). Neither fit describes the full range well, and the $f_{\rm H\,I}(N, X)$ shows a flattening near the canonical DLA definition of $\log N_{\rm H\,I} = 20.3$ cm^{-2}. [*See the electronic edition of the Journal for a color version of this figure.*]

fractionally larger $g(z)$ at those redshifts. Although the mean differs by only $\delta z = 0.3$, we note that the comparison is not perfect as we have not considered any evolution in the normalization of $f_{\rm H\,I}(N, X)$ for the SLLS or DLA but have simply plotted the full samples. Another systematic effect is that the SDSS DLA sample may suffer from a Malmquist bias. Specifically, the statistical and systematic errors (e.g., the effects of line blending) in the $N_{\rm H\,I}$ values of the DLA are significant and will drive the observed $f_{\rm H\,I}(N, X)$ distribution to a steeper slope. It is possible that this effect explains the marked drop in $f_{\rm H\,I}(N, X)$ at $N_{\rm H\,I} = 10^{20.7}$ cm^{-2} in Figure 8. We intend to address this issue directly with follow-up, higher resolution observations of a large sample of SDSS DLAs with $N_{\rm H\,I} \approx 10^{20.3}$ cm^{-2}. If there is a substantial Malmquist bias in the DLA sample, then the decrease in the slope of $f_{\rm H\,I}(N, X)$ would be more gradual than that suggested by Figure 8.

4.4. *Is There an Inflection in $f_{\rm H\,I}(N, X)$ within the SLLS Range?*

While the mismatch between the DLA and the Lyα forest in the power-law description of their $f_{\rm H\,I}(N, X)$ distributions suggests that $f_{\rm H\,I}(N, X)$ for the LLS will show intermediate values ($\alpha \approx -1.7$), the observed incidence of LLSs reveals a different result. As PHW05 discussed, a simple spline interpolation of the DLA and Lyα forest $f_{\rm H\,I}(N, X)$ distributions through the LLS regimes predicts over an order of magnitude more LLSs than observed per ΔX. PHW05 argued, therefore, that the $f_{\rm H\,I}(N, X)$ distribution for the LLS must exhibit an inflection as evidenced by $d \log f/d \log N > -1.5$. Zheng & Miralda-Escudé (2002) have also predicted that there should be an inflection in $f_{\rm H\,I}(N, X)$ in the SLLS regime for galaxies exposed to an ionizing radiation field. It is worth investigating with our data set whether evidence exists for just such an inflection.

The simplest approach is to examine whether $d \log f/d \log N > -1.5$ in the LLS regime. Regarding our results on the SLLS, we find that $d \log f/d \log N > -1.5$ for both the $\log N_{\rm H\,I}^{\rm lim} = 19.0$ cm^{-2} and $\log N_{\rm H\,I}^{\rm lim} = 19.3$ cm^{-2} groups (Table 5). The differences, however, have less than 2 σ significance. Using only the current data set and the distribution of DLAs, we do not report the existence of an inflection in $f_{\rm H\,I}(N, X)$ within the SLLS regime.

4.4.1. *Constraints from lower $N_{\rm H\,I}$ LLSs*

In order to pursue the question further, we introduce two new observational constraints on the LLS. The statistical significance for the SLLS alone is limited by the combination of sample size and observed baseline in $\log N_{\rm H\,I}$. We cannot arbitrarily increase the sample size, but we are able to introduce new constraints that are sensitive to lower column density LLSs. The number density of optically thick LLSs has been well constrained by many studies. For our purposes here, we apply the constraint at redshift $z = 3$ of $\ell(X)_{\rm LLS} = 0.7 \pm 0.1$ (Sargent et al. 1989; Storrie-Lombardi et al. 1994; Péroux et al. 2003b). We also use a measure of the incidence of optically thin partial Lyman limit systems (PLLSs) from Burles (1997), who found 12 systems with mean redshift at $z = 3$ with 17.2 cm^{-2} $< \log N_{\rm H\,I} <$ 17.8 cm^{-2} over a redshift path of $\Delta z_{\rm PLLS} = 59.07$ and absorption path of $\Delta X_{\rm PLLS} = 16.63$. This gives $\ell(X)_{\rm PLLS} = 0.20 \pm 0.06$.

4.4.2. *The Observable Distribution Function $\mathcal{O}(N, X)$*

In order to facilitate the analysis and interpretation of the distribution over the full range of LLSs and DLAs, we introduce a function called the observable distribution function of H I:

$$\mathcal{O}(N, X) = \frac{m}{\Delta \log N \Delta X} = \frac{\ell(X)}{\Delta \log N}, \qquad (5)$$

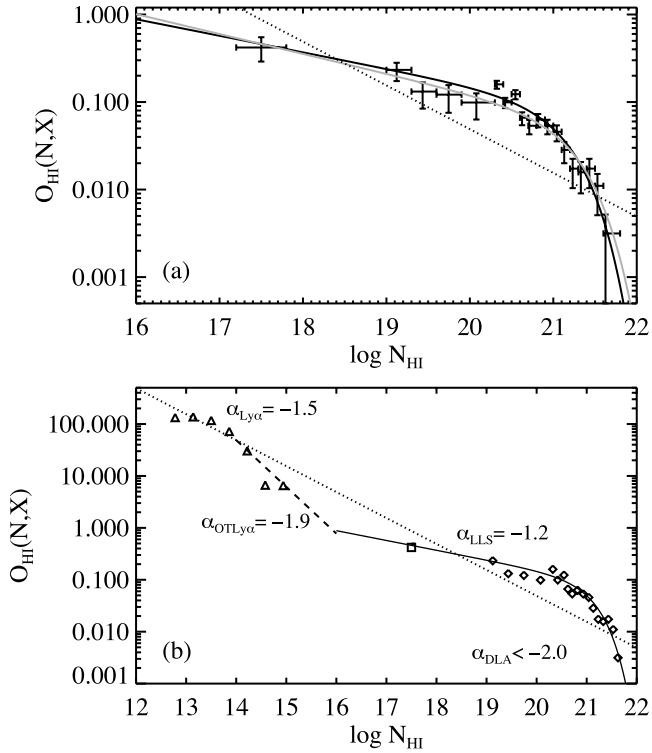

FIG. 9.—(*a*) Values for the observable distribution function for the entire range of H I absorbers that are optically thick at the Lyman limit. The solid line is a best-fit three-parameter function (assuming Gaussian statistics) of the data, which include the SLLSs presented here, the DLAs from PHW05, and a bin that contains the constraint on the number of partial LLSs. The dot-dashed line shows the best fit after removing the two outlying bins from the PHW sample. Also shown (*dotted line*) is the $\mathcal{O}(N, X)$ for the Lyα forest. (*b*) Same as (*a*), but extended to include the Lyα forest results of Kirkman & Tytler (1997), which are shown as triangles. The constraint from the number of partial LLSs is displayed by the square. Overlaid are the values for the power-law slope α for the $N_{\rm H\,I}$ regions, $\alpha_{\rm Ly\alpha}$ corresponding to the optically thin Lyα forest with $12.1 < \log N_{\rm H\,I} < 14$, $\alpha_{\rm OT\,Ly\alpha}$ corresponding to the optically thick Lyα forest with $14 < \log N_{\rm H\,I} < 16$, $\alpha_{\rm LLS}$ corresponding to $16 < \log N_{\rm H\,I} < 20.3$, and $\alpha_{\rm DLA}$ corresponding to $\log N_{\rm H\,I} = 20.3$–21.3, to highlight the observed and predicted changes in the logarithmic slope of $f_{\rm H\,I}(N, X)$. [*See the electronic edition of the Journal for a color version of this figure.*]

where m is the number of systems observed over an absorption path, ΔX, and a column density range $\Delta \log N$. This is simply the frequency distribution function in logarithmic column density bins and is related to the classic distribution by

$$\mathcal{O}(N, X) d \log N = f(N, X)\, dN,$$
$$\mathcal{O}(N, X) = f(N, X) N \ln(10). \qquad (6)$$

The observable distribution has a few nice features. It is unitless and gives the direct number of systems observed over a specified bin in logarithmic column density (almost all studies of H I absorption show and analyze the data in bins of constant width in $\log N_{\rm H\,I}$). It also removes one factor of column density from the steep slope in the frequency distribution, which enables better assessments of change in slopes, as well as smaller effects from the rapid change in the distribution over bins of large size.

4.4.3. *$\mathcal{O}(N, X)$ for the LLSs and the DLAs*

In Figure 9 we show the observational constraints on $\mathcal{O}(N, X)$ from the present sample of SLLSs and the DLAs from PHW05. In addition, we show an observational constraint on the abundance of partial Lyman limits at $z = 3$, $\mathcal{O}_{\rm PLLS} = 0.42 \pm 0.13$,

corresponding to the column density interval (17.2 cm^{-2} < $\log N_{\rm H\,I}$ < 17.8 cm^{-2}; Burles 1997).

We fit a simple analytic function to the combined set of ALL-19.0 SLLSs (Table 5), the PHW05 DLA sample for $\log N_{\rm H\,I} >$ 20.3 cm^{-2}, as well as the two additional LLS constraints described above. We fit a three-parameter model expressed as

$$\log \mathcal{O}(N, X) = a + b(\log N_{\rm H\,I} - 19) - 10^{\log N_{\rm H\,I} - c}. \quad (7)$$

This parameterized form can be recast into a more familiar Γ-distribution (e.g., Pei & Fall 1995; Péroux et al. 2003b):

$$\mathcal{O}(N, X) = \mathcal{O}_0 \left(\frac{N_{\rm H\,I}}{N_*}\right)^{\alpha+1} e^{-N_{\rm H\,I}/N_*}, \quad (8)$$

where $\log N_* = c - 0.3622$, $\log \mathcal{O}_0 = b \log N_* + (a - 19b)$, and $\alpha = b - 1$.

We show the best-fit function to the binned data assuming Gaussian statistics as the solid line in Figure 9, parameterized by $(a, b, c) = (-0.621, -0.189, 21.51)$, which gives a reduced χ^2 for 17 degrees of freedom (dof), $\chi^2_\nu = 1.86$. We assess the dependence of the fitting on the included data sets, by sequentially removing constraints. If we do not include the constraint on the total number of optically thick Lyman limits, the best-fit parameters are virtually unchanged, and the fitted parameters above give a predicted number of optically thick Lyman limits of $\ell(X)^{\rm fit}_{\rm LLS} = 0.68$. The two outliers in the above fit are the DLA points centered near bins of $\log N_{\rm H\,I} = 20.3$ and 20.6 cm^{-2}. If we drop the first of these points, we find (−0.660, −0.198, 21.56) and $\chi^2_\nu = 1.24$ for 15 dof. Dropping both DLA bins gives an acceptable fit, with (−0.677, −0.227, 21.63) and $\chi^2_\nu = 0.552$ for 14 dof. The last fit is shown as a dot-dashed line in Figure 9.

The fits show that the $\mathcal{O}(N, X)$ slope in the SLLS region falls between $-0.227 < b < -0.189$ (recall $\alpha = b - 1$). We also find that the H I cutoff scale is between $21.51 < c < 21.63$, which matches the results of PHW05 and Péroux et al. (2003b). All of the fits produce a reasonable number of optically thick LLSs: $0.61 < \ell_{\rm LLS}(X) < 0.68$.

4.4.4. *Are the SLLSs a Distinct Population?*

Finally, we present another moment of the $N_{\rm H\,I}$ distribution, $N_{\rm H\,I}\mathcal{O}(N, X)$, in Figure 10. This represents the total H I column density per unit logarithmic column density per unit absorption path. The SLLS and DLA data points and the first analytic fit (to the entire data set) are shown. The data are relatively flat from $N_{\rm H\,I} = 10^{20.3}$ to $10^{21.5}$ cm^{-2} with the functional form peaking at $\log N_{\rm H\,I} = 21.1$. It is evident that absorbers with $N_{\rm H\,I} \approx 10^{21}$ cm^{-2} dominate the mass density of H I in the universe. Consider a comparison of the SLLSs and DLAs. Whereas the DLAs with $20.3 < \log N_{\rm H\,I} < 21.5$ dominate the mass density with roughly equal contribution per $\Delta \log N$, the SLLSs lie distinctly below, with the absorbers at $N_{\rm H\,I} = 10^{19}$ cm^{-2} adding a negligible portion and the full SLLS range in $N_{\rm H\,I}$ contributing only ≈15% to the total mass density. We note that Zwaan et al. (2005) obtain a very similar shape for $N_{\rm H\,I}\mathcal{O}(N, X)$ at $z = 0$. Again, this behavior is likely related to the fact that the majority of SLLSs are highly ionized. The results in Figure 10 lend further support to the concept that the SLLS absorbers are a distinct population from the DLAs.

4.5. *Implications for Lower $N_{\rm H\,I}$*

Armed with a description for the full range of H I column densities that are optically thick at the Lyman limit, we now wish to extend our analysis downward in $N_{\rm H\,I}$ to the Lyα forest. Although a more thorough analysis is required to fully assess the statistically acceptable distributions over such a large range in $\log N_{\rm H\,I}$, we can clearly show that slopes in the SLLS region as steep as $\alpha = -1.5$ are unacceptable. In Figure 9*b* we overplot the extrapolation of the best-fit observable distribution of low column density Lyα absorbers ($12.1 < \log N_{\rm H\,I} < 14$) as a dotted line with a slope of $b = -0.5$ [i.e., $f_{\rm H\,I}(N, X) \propto N^{-1.5}$; Kirkman & Tytler 1997]. Although the extrapolation has uncertainties related to the normalization and completeness, it does highlight the overprediction of SLLSs based on a simple power-law extrapolation from lower column density studies. Even if we allowed for freedom in normalization, it is clear that in no region except near $\log N_{\rm H\,I} = 20.5$ cm^{-2} is $\alpha = -1.5$ a good description of the high $\log N_{\rm H\,I}$ distribution. A subset of the data that were used to constrain the fit to Lyα absorbers is shown in Figure 9*b* as triangles.[11] A gamma function with low-end slope of $\alpha = -1.2$ is a good fit to the high-density data sets of LLSs and DLAs. But the extrapolation of the low-end slope to the regime of the Lyα absorbers underpredicts the observed numbers by almost a factor of 100!

In order to reconcile the data presented here, together with the DLAs, LLSs, and the Lyα absorbers, the full distribution function must contain at least three changes in logarithmic slope of the frequency distribution (or inflections, $d^2f/dN^2 = 0$), as previously argued (in part) by Bechtold (1987) and Petitjean et al. (1993). The first inflection is seen in the change between the DLA distribution and SLLSs. This is required if one includes constraints from the LLSs and the PLLSs and demands constant slopes down to these column densities. There must then be at least two more changes in the logarithmic slopes, one to account for the much higher number of Lyα absorbers, and the second to finally merge back to the Lyα slope with $\alpha = -1.5$. We present one such solution with a dotted line bridging the gap between $\log N_{\rm H\,I} = 14$ cm^{-2} and $\log N_{\rm H\,I} = 16$ cm^{-2} with a frequency slope of $\alpha = -1.9$. The Lyα absorbers are claimed to have a single power-law slope over two decades of $N_{\rm H\,I}$ (12.5 cm^{-2} < $\log N_{\rm H\,I}$ < 14.5 cm^{-2}) and are classified as a single population.

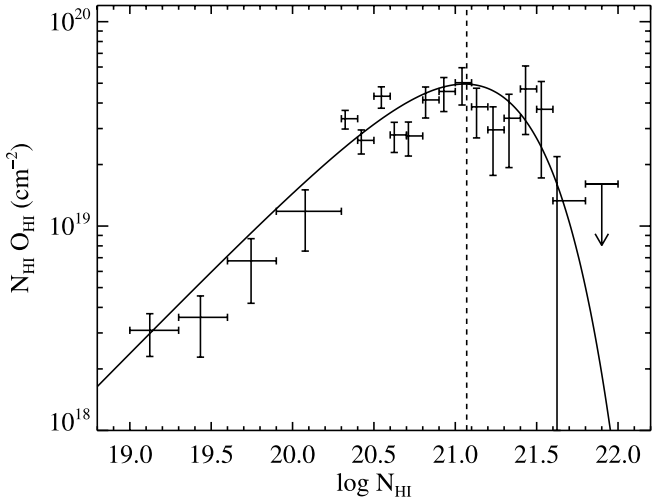

FIG. 10.—Values for $N_{\rm H\,I}\mathcal{O}(N, X)$, the first moment of the observable distribution function over the SLLS and DLA range. The data give the relative contributions to the cosmic density of hydrogen atoms per unit $\log N_{\rm H\,I}$ at $z \sim 3$ and show that DLAs with $\log N_{\rm H\,I} = 20.3$–21.5 overwhelmingly dominate the H I mass density, with the SLLSs contributing only ≈15% to the total.

[11] Note that the two points above $\log N_{\rm H\,I} = 14.5$ cm^{-2} were not included in the power-law fit.

In comparison, the absorbers spanning 17 $cm^{-2} < \log N_{H\,I} <$ 20 cm^{-2}, over three decades of $N_{H\,I}$, are well described by a single power-law slope of $\alpha = -1.2$ and also could be classified as a single population by applying the same argument.

5. CONCLUDING REMARKS

The SLLS results presented in this paper motivate several avenues of future exploration. First, we must extend the survey downward in LLS H I column density. An improved constraint on the number of optically thick LLSs would significantly tighten the constraint on the low-end slope of the SLLS distribution. Second, a large sample of higher H I column density Lyα forest data is needed. Specifically, a large sample of Lyα forest with 14.5 $cm^{-2} \leq \log N_{H\,I} \leq 16.5$ cm^{-2} directly tests the predicted shape of the H I distribution. Finally, one must pursue detailed ionization studies of the LLS to fully assess their baryonic mass, metallicity, etc. Our survey will provide the data set required for just such studies.

This paper includes data gathered with the 6.5 m Magellan Telescopes located at Las Campanas Observatory, Chile. The authors wish to recognize and acknowledge the very significant cultural role and reverence that the summit of Mauna Kea has always had within the indigenous Hawaiian community. We are most fortunate to have the opportunity to conduct observations from this mountain. J. O. and S. B. acknowledge support from NSF grant AST 03-07705. G. E. P. and J. X. P. are supported by NSF grant AST 03-07408.

REFERENCES

Adelman-McCarthy, J. K., et al. 2006, ApJS, 162, 38
Bahcall, J. N., & Peebles, P. J. E. 1969, ApJ, 156, L7
Bechtold, J. 1987, in High Redshift and Primeval Galaxies, ed. J. Bergeron et al. (Gif-sur-Yvette: Editions Frontières), 397
Bennett, C. L., et al. 2003, ApJS, 148, 1
Bernstein, R., Shectman, S. A., Gunnels, S. M., Mochnacki, S., & Athey, A. E. 2003, Proc. SPIE, 4841, 1694
Bouché, N., Lehnert, M. D., & Péroux, C. 2006, MNRAS, 367, L16
Burles, S., & Tytler, D. 1998, ApJ, 507, 732
Burles, S. M. 1997, Ph.D. thesis, Univ. California, San Diego
Cristiani, S., D'Odorico, S., Fontana, A., Giallongo, E., & Savaglio, S. 1995, MNRAS, 273, 1016
Croft, R. A. C., Weinberg, D. H., Bolte, M., Burles, S., Hernquist, L., Katz, N., Kirkman, D., & Tytler, D. 2002, ApJ, 581, 20
Dekker, H., D'Odorico, S., Kaufer, A., Delabre, B., & Kotzlowski, H. 2000, Proc. SPIE, 4008, 534
Dessauges-Zavadsky, M., Péroux, C., Kim, T.-S., D'Odorico, S., & McMahon, R. G. 2003, MNRAS, 345, 447
Kim, T.-S., Carswell, R. F., Cristiani, S., D'Odorico, S., & Giallongo, E. 2002, MNRAS, 335, 555
Kirkman, D., & Tytler, D. 1997, ApJ, 484, 672
Kirkman, D., Tytler, D., Suzuki, N., O'Meara, J. M., & Lubin, D. 2003, ApJS, 149, 1
Lanzetta, K. M. 1991, ApJ, 375, 1
———. 1993, in The Environment and Evolution of Galaxies, ed. J. M. Shull & H. A. Thronson (Dordrecht: Kluwer), 237
McDonald, P., et al. 2005, ApJ, 635, 761
Pei, Y. C., & Fall, S. M. 1995, ApJ, 454, 69
Péroux, C., Dessauges-Zavadsky, M., D'Odorico, S., Kim, T.-S., & McMahon, R. G. 2003a, MNRAS, 345, 480
Péroux, C., Dessauges-Zavadsky, M., D'Odorico, S., Sun Kim, T., & McMahon, R. G. 2005, MNRAS, 363, 479
Péroux, C., Kulkarni, V. P., Meiring, J., Ferlet, R., Khare, P., Lauroesch, J. T., Vladilo, G., & York, D. G. 2006, A&A, 450, 53
Péroux, C., McMahon, R. G., Storrie-Lombardi, L. J., & Irwin, M. J. 2003b, MNRAS, 346, 1103
Petitjean, P., Webb, J. K., Rauch, M., Carswell, R. F., & Lanzetta, K. 1993, MNRAS, 262, 499
Prochaska, J. X. 1999, ApJ, 511, L71
Prochaska, J. X., Gawiser, E., Wolfe, A. M., Cooke, J., & Gelino, D. 2003, ApJS, 147, 227
Prochaska, J. X., & Herbert-Fort, S. 2004, PASP, 116, 622
Prochaska, J. X., Herbert-Fort, S., & Wolfe, A. M. 2005, ApJ, 635, 123 (PHW05)
Prochaska, J. X., O'Meara, J. M., Herbert-Fort, S., Burles, S., Prochter, G. E., & Bernstein, R. A. 2006, ApJ, 648, L97
Prochaska, J. X., & Wolfe, A. M. 1999, ApJS, 121, 369
Sargent, W. L. W., Steidel, C. C., & Boksenberg, A. 1989, ApJS, 69, 703
Sheinis, A. I., Bolte, M., Epps, H. W., Kibrick, R. I., Miller, J. S., Radovan, M. V., Bigelow, B. C., & Sutin, B. M. 2002, PASP, 114, 851
Sheth, R. K., & Tormen, G. 1999, MNRAS, 308, 119
Steidel, C. C. 1990, ApJS, 74, 37
Stengler-Larrea, E. A., et al. 1995, ApJ, 444, 64
Storrie-Lombardi, L. J., McMahon, R. G., Irwin, M. J., & Hazard, C. 1994, ApJ, 427, L13
Tytler, D. 1982, Nature, 298, 427
Tytler, D., et al. 2004, ApJ, 617, 1
Viegas, S. M. 1995, MNRAS, 276, 268
Wolfe, A. M., Gawiser, E., & Prochaska, J. X. 2005, ARA&A, 43, 861
Zheng, Z., & Miralda-Escudé, J. 2002, ApJ, 568, L71
Zwaan, M. A., van der Hulst, J. M., Briggs, F. H., Verheijen, M. A. W., & Ryan-Weber, E. V. 2005, MNRAS, 364, 1467